



ELSEVIER

Contents lists available at ScienceDirect

## Journal of Magnetism and Magnetic Materials

journal homepage: [www.elsevier.com/locate/jmmm](http://www.elsevier.com/locate/jmmm)

# On-chip magnetic bead-based DNA melting curve analysis using a magnetoresistive sensor



Giovanni Rizzi, Frederik W. Østerberg, Anders D. Henriksen, Martin Dufva, Mikkel F. Hansen\*

Department of Micro- and Nanotechnology, Technical University of Denmark, DTU Nanotech, Building 345 East, DK-2800 Kongens Lyngby, Denmark

## ARTICLE INFO

## Article history:

Received 27 June 2014

Accepted 2 September 2014

Available online 11 September 2014

## Keywords:

Single nucleotide polymorphism

DNA analysis

Magnetoresistive sensor

Magnetic biosensor

Planar Hall effect

Lab-on-a-chip

## ABSTRACT

We present real-time measurements of DNA melting curves in a chip-based system that detects the amount of surface-bound magnetic beads using magnetoresistive magnetic field sensors. The sensors detect the difference between the amount of beads bound to the top and bottom sensor branches of the differential sensor geometry. The sensor surfaces are functionalized with wild type (WT) and mutant type (MT) capture probes, differing by a single base insertion (a single nucleotide polymorphism, SNP). Complementary biotinylated targets in suspension couple streptavidin magnetic beads to the sensor surface. The beads are magnetized by the field arising from the bias current passed through the sensors. We demonstrate the first on-chip measurements of the melting of DNA hybrids upon a ramping of the temperature. This overcomes the limitation of using a single washing condition at constant temperature. Moreover, we demonstrate that a single sensor bridge can be used to genotype a SNP.

© 2014 Elsevier B.V. All rights reserved.

## 1. Introduction

Magnetic beads have the advantage over, e.g., fluorescent tags that virtually all biological and chemical samples do not exhibit significant magnetic properties and hence that there is no magnetic signal background from the sample matrix. In addition, the development of magnetoresistive sensor technology for read heads in hard disk drives has spawned extensive interest in the use of magnetoresistive sensors for magnetic biosensing [1–5].

DNA microarrays have revolutionized the analysis of genetic mutations related to disease diagnostics and a single microarray can be used to analyze up to 10,000 locations in the genome [6]. Microarrays rely on allele specific hybridization, where the fluorescently tagged target hybridizes to a set of surface-bound capture probes matching the wild type (WT) and mutant type (MT) variants of the gene of interest. The fluorescence from the set of microarray spots for a given gene can, after a washing step where weakly bound targets are washed off, be used to determine the types of the gene that are present in the sample (genotyping) by using a microarray laser scanner. To obtain a reliable genotyping, it is important to choose a combination of capture probe lengths and washing conditions that enable a clear distinction between matching and mismatching probe–target hybrids and for single nucleotide polymorphisms (SNPs), where

the MT type target differs from the WT target by a single base, this can be challenging [7]. SNP genotyping is therefore often carried out in a homogeneous format, where the melting of DNA hybrids (giving a fluorescent signal) is investigated as function of temperature and the presence of a SNP can be observed as a temperature shift in the melting curve. However, such measurements only allow for a limited set of probes to be investigated.

Magnetoresistive sensors have the potential to be used for the investigation of the magnetic bead binding to a large set of capture probes [8] and may moreover provide a compact and relatively inexpensive set-up suited for use outside a specialized laboratory setting [9]. Sensors based on the giant magnetoresistance effect have previously been used to detect DNA by several groups – usually by detecting the signals due to magnetic beads bound to sensors functionalized with capture probes after incubation and washing [2,3,10,11]. Although on-chip magnetic field generators have been presented [12], the magnetic beads are usually magnetized using an external electromagnet [13–15]. In our previous work, we have demonstrated the detection of surface-bound magnetic beads to the so-called planar Hall effect bridge (PHEB) magnetoresistive sensors using only the magnetic field due to the sensor bias current required to excite the magnetic beads, thus eliminating the need for external electromagnets. Moreover, using a differential sensor geometry, we have recently demonstrated the detection of a SNP from the real-time sensor signals measured during and after a single washing step [16].

Here, we expand on our previous work by providing the first demonstration of on-chip measurements of DNA melting curves

\* Corresponding author.

E-mail addresses: [giori@nanotech.dtu.dk](mailto:giori@nanotech.dtu.dk) (G. Rizzi), [mikkel.hansen@nanotech.dtu.dk](mailto:mikkel.hansen@nanotech.dtu.dk) (M.F. Hansen).

using a ramping of the temperature. To obtain reliable results, it is essential to properly correct the temperature dependence of the sensor and magnetic bead parameters and we therefore give a detailed presentation of the data treatment procedure. Finally, we show for the first time that a single sensor bridge functionalized with WT and MT probes on the two sensor halves can be used for the genotyping of a SNP.

## 2. Theory

The sensor geometry is shown in Fig. 1 and comprises four segments of the magnetoresistive stack arranged in a Wheatstone bridge geometry. When a low uniform magnetic field  $H_y$  is applied to the sensor in the  $y$ -direction, the resistance of each sensor arm is

$$R\left(\alpha = \pm \frac{\pi}{4}, H_y\right) = R_0 \mp S_0 H_y \quad (1)$$

where  $\alpha$  is the angle that each bridge arm forms with the  $x$ -axis,  $R_0$  is the resistance of the arm in zero magnetic field and  $S_0$  is the low-field sensitivity [16]. When the bridge is biased by a voltage  $V_x$ , a variation of the resistances results in an output voltage  $V_y$  from the Wheatstone bridge. Moreover, when the sensor is biased with a voltage  $V_x = \sqrt{2} V_{\text{RMS}} \sin(2\pi ft)$ , where  $V_{\text{RMS}}$  is the root mean square (RMS) amplitude of the voltage and  $f$  is the frequency, the current running in the sensor arms generates a small alternating magnetic field in the proximity of the sensor surface [17,18]. This self-field magnetizes magnetic beads in the vicinity of the sensor that give rise to an average magnetic field  $H^{\text{sf}} = \gamma I_{\text{arm}}$  acting perpendicular to the arm, where  $I_{\text{arm}}$  is the current in the arm and  $\gamma$  depends on the amount and distribution of magnetic beads as well as the sensor geometry [16,17,19]. In addition to a contribution from magnetic beads, partial shunting of the sensor bias current in the antiferromagnet results in a sensor self-biasing, which is nominally eliminated in the differential PHEB (dPHEB) geometry of Fig. 1 [19]. The detection of magnetic beads using the sensor self-field eliminates the need for externally applied magnetic fields. The bead signal can be measured in the second harmonic out-of-phase lock-in signal, which for the dPHEB geometry can be written as [16]

$$V_2^* = -\frac{1}{8} S_0(T) \left(\frac{V_{\text{RMS}}}{R_0(T)}\right)^2 (\gamma_{\text{top}} - \gamma_{\text{bottom}}) + V_0(T) \quad (2)$$

where  $\gamma_{\text{top}}$  and  $\gamma_{\text{bottom}}$  depend on the amount of beads present over the top and bottom halves of the sensor bridge and  $V_0$  is introduced to account for an offset in the second harmonic out-of-phase signal that would be zero for a perfectly balanced bridge. As discussed by Rizzi et al. [16], Eq. (2) shows that the bead contributions from top and bottom arms cancel out in a uniform bead background. When only the top half of the sensor is functionalized with capture probes, this allows to cancel out the signal from beads in uniform suspension over the sensor. Moreover, in the present work, the top and bottom halves of the sensor will be functionalized with two different capture probes to directly obtain the differential binding signal between the two probes.

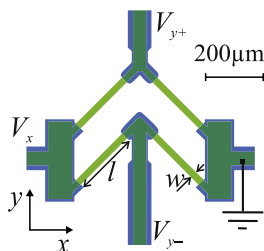


**Fig. 1.** Illustration of the dPHEB sensor geometry. The sensor is voltage biased along the  $x$ -axis and the voltage output  $V_y$  is measured along the  $y$ -axis. All sensors of the present study had  $l = 250 \mu\text{m}$  and  $w = 25 \mu\text{m}$ .

The signal  $V_2^*$  shows a non-trivial dependence on temperature. The low-field sensitivity  $S_0(T)$  depends on temperature ( $T$ ) and increases up to 10% when the temperature is ramped from room temperature to  $70^\circ\text{C}$  and the increased temperature may also induce irreversible changes [20]. Moreover, the sensor offset  $V_0(T)$  and the resistance  $R_0(T)$  also vary with temperature. The terms  $\gamma_{\text{top}}$  and  $\gamma_{\text{bottom}}$  depend on the temperature stability of the binding of the magnetic beads as well as on the temperature dependent magnetic properties of the beads. Properly corrected as we will show below, however, the  $V_2^*$  data can be used to determine the stability of the binding of the magnetic beads with minimum influence from the other temperature dependent parameters.

## 3. Materials and methods

### 3.1. Sensor fabrication

The sensors of Fig. 1 with  $l = 250 \mu\text{m}$  and  $w = 25 \mu\text{m}$  were fabricated as described previously [16,21]. Briefly, the top-pinned magnetic stack Ta(5)/Ni<sub>80</sub>Fe<sub>20</sub>(30)/Mn<sub>80</sub>Ir<sub>20</sub>(10)/Ta(5) (thicknesses in nm) was sputter deposited. The easy axis of magnetization was defined during deposition by applying a saturating magnetic field along the  $x$ -axis. The electrical contacts of Ti(10)/Pt(100)/Au(100)/Ti(10) were deposited by electron beam evaporation. The sensors were passivated as described by Rizzi et al. [16] with a spin coated hybrid polymer (Ormocomp, Micro Resist Technology, GmbH, Germany) of thickness 900 nm. The wafer was diced into chips, each comprising six magnetic field sensors.

### 3.2. Surface functionalization

The allele specific DNA capture probes were covalently linked to the sensor surface through a silanization of the protective sensor coating as described by Rizzi et al. [16]. The DNA capture probes used in this work were designed by Petersen et al. [22] for SNP genotyping of the human beta globin (HBB) gene. The probes (sequences given in [16]) were purchased from DNA technology A/S, Denmark. Here, probes designed for the CD 8/9 mutation site were selected as a model system. The wild type (WT) and mutant type (MT) probes differ by a single base insertion. In addition, we used a biotinylated capture probe linked to the surface of a positive reference sensor to provide a direct linking of the streptavidin magnetic beads to the sensor surface. The capture probes were spotted over four dPHEB sensors as depicted in Fig. 2 using a Nanoplotter with a Nanotip (GeSim GmbH, Germany). The sensor surface was blocked prior to use in a solution of 1 mg/mL bovine serum albumin in  $1 \times$  phosphate buffered saline (PBS) for 20 min. The sensors will be named according to the probe used for functionalization (e.g., ‘WT sensor’ refers to the sensor functionalized with the WT capture probe).

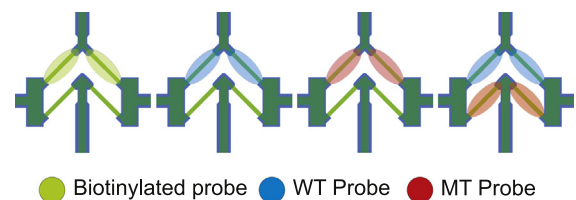


**Fig. 2.** Probe patterning for temperature denaturation studies. Sensors are functionalized with WT and MT DNA capture probes. A biotinylated capture probe provides a direct binding site for magnetic beads over the positive reference sensor.

### 3.3. Measurement platform

The measurement setup used here was described in detail by Österberg et al. [23] and Rizzi et al. [16]. Briefly, the chip was mounted in a click-on microfluidic system that both provided electrical contact to each sensor and defined a fluidic channel ( $1 \times 1 \times 5 \text{ mm}^3$ ) over the sensor surface.

The sensor response to magnetic beads was measured in the second harmonic out-of-phase lock-in signal using a SR830 lock-in amplifier with a SR552 voltage preamplifier, both from Stanford Research Systems, Inc., USA. All signals are corrected for the pre-amplification factor. The driving signal, provided by the lock-in amplifier, was amplified using a commercial audio amplifier to drive all sensors on a chip in parallel with a voltage of  $V_{\text{RMS}} = 1.6 \text{ V}$  at a frequency  $f = 167 \text{ Hz}$ .

The temperature of the sensor mount in good thermal contact to the sensor chip was measured using a Pt1000 thermoresistor. The temperature was controlled via a LFI3751 control unit (Wave-length Electronics, USA) driving a Peltier element. The temperature control system achieved an accuracy of  $0.1 \text{ }^\circ\text{C}$  and the temperature ramping was software controlled.

### 3.4. Experimental procedure

#### 3.4.1. Reference measurements

Prior to hybridization with target DNA, the temperature dependence of the second harmonic out-of-phase signal offset was characterized. For this, the sensors were washed with  $0.05 \times \text{SSC}$  ( $c(\text{Na}^+) = 10 \text{ mM}$ ) and left stagnant. Subsequently, the second harmonic out-of-phase signal was measured during a linear temperature ramping from  $20 \text{ }^\circ\text{C}$  to  $70 \text{ }^\circ\text{C}$  and back to  $20 \text{ }^\circ\text{C}$  at  $0.1 \text{ }^\circ\text{C/s}$ .

#### 3.4.2. Hybridization and denaturation

The biotinylated wild type (WT) DNA target (sequence given in [16]) was diluted and mixed 1:1 v:v with stock solution of Miltenyi Streptavidin MicroBeads (Miltenyi Biotec Norden AM, Sweden) with a nominal diameter of  $50 \text{ nm}$ . The final oligonucleotide concentration was  $5 \text{ nM}$  in  $2 \times \text{SSC}$  corresponding to  $c(\text{Na}^+) = 400 \text{ mM}$ . The sample was incubated at  $37 \text{ }^\circ\text{C}$  for  $30 \text{ min}$ . The hybridization reaction was then inhibited by lowering the temperature to  $20 \text{ }^\circ\text{C}$ . Subsequently, the unbound target and unbound magnetic beads were washed with  $0.05 \times \text{SSC}$  ( $c(\text{Na}^+) = 10 \text{ mM}$ ) for  $80 \text{ s}$  at a flow rate of  $30 \text{ } \mu\text{L/min}$ .

Following hybridization and washing of unbound target and beads, the DNA hybrids were denatured by increasing the temperature. For this purpose, the sensor signal was measured during ramping up the temperature ( $V_{\text{up}}(T)$ ) from  $20 \text{ }^\circ\text{C}$  to  $70 \text{ }^\circ\text{C}$  at  $0.1 \text{ }^\circ\text{C/s}$ . After denaturation of the hybrids, a reference measurement  $V_{\text{down}}(T)$  was taken while ramping the temperature back down to  $20 \text{ }^\circ\text{C}$  at  $0.1 \text{ }^\circ\text{C/s}$ .

### 3.5. Data treatment

To correct for the temperature dependence of the signal offset, a reference measurement of  $V_0(T)$  for the positive reference sensor was performed prior to bead binding. For the other sensors, the measurements performed while ramping the temperature down after melting were used as references for the sensor offsets, i.e., for those sensors  $V_0(T) = V_{\text{down}}(T)$ . For all sensors, a second order polynomial fit to the  $V_0(T)$  data was subtracted from the sensor signal to obtain  $\Delta V = V_2^*(T) - V_0(T)$ . To correct for the temperature dependence of the sensor sensitivity and the bead response, the signals  $\Delta V$  for all sensors were normalized by the positive

reference signal to obtain

$$\text{Relative Signal} = \Delta V(T) / \Delta V_{\text{ref}}(T). \quad (3)$$

## 4. Results and discussion

In this section, we present results from hybridization and temperature denaturation assays on the dPHEB sensors. First, we present the signal from magnetic beads obtained during hybridization of the sensors with a WT DNA target and streptavidin magnetic beads. Then, the sensor signals measured as function of increasing temperature will be presented and corrected for the known temperature dependencies of the sensor output.

### 4.1. Hybridization signal

Biotinylated WT DNA target and magnetic beads were mixed in 1:1 v:v ratio to a final concentration  $c = 5 \text{ nM}$  of oligonucleotides in  $2 \times \text{SSC}$ . The sample was incubated over the sensor at  $37 \text{ }^\circ\text{C}$  for  $30 \text{ min}$ . Fig. 3 shows the variation of the second harmonic out-of-phase signal  $\Delta V_2^*(t) = V_2^*(t) - V_2^*(0)$  as a function of time ( $t$ ) for the four sensors during hybridization with the WT target–streptavidin magnetic bead mixture. The sample was injected at time  $t=0 \text{ s}$ . The signal from the positive reference sensor, where streptavidin coated beads can directly link to the biotinylated capture probes, increased rapidly and approached saturation after  $15 \text{ min}$ . In this situation, with an excess of magnetic beads, the binding sites over the sensor surface are saturated. The signal from the positive reference sensor is therefore the maximum signal achievable with this capture probe surface density.

The signals from both the WT and MT sensors increased steadily during the hybridization at a significantly slower rate than the positive reference sensor. The WT sensor reached about half the signal from the positive reference sensor after  $30 \text{ min}$  of hybridization. The MT sensor signal increased at a lower rate than that from the WT sensor. To promote the formation of DNA duplexes, a low-stringency condition ( $c(\text{Na}^+) = 400 \text{ mM}$ ) was used during hybridization. This allowed the formation of mismatched hybrids between WT target and MT probes, although with a reduced rate. The signal from the differential sensor functionalized with both MT and WT capture probes (the WT–MT sensor) increased slightly during the hybridization confirming a faster hybridization rate for the perfectly matched hybrids between WT target and WT probes.

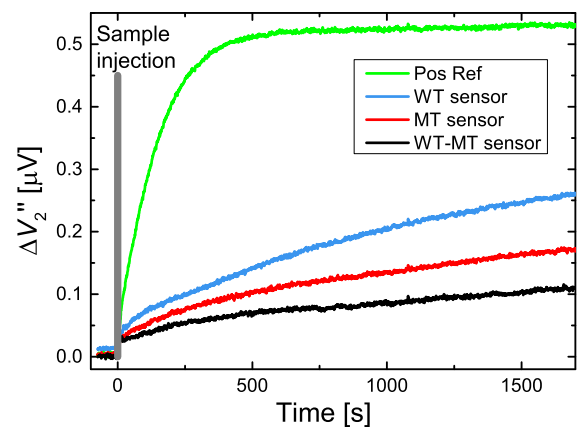
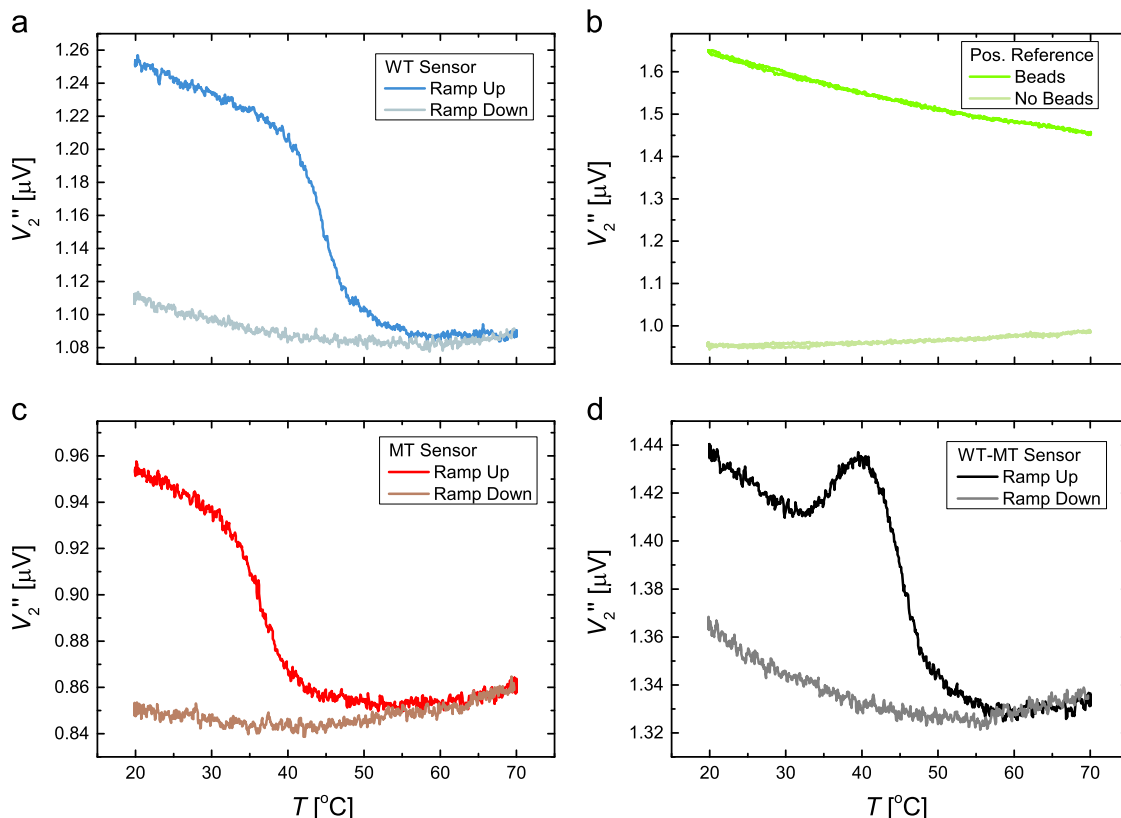


Fig. 3. Second harmonic out-of-phase sensor signal variation  $\Delta V_2^*(t)$  measured during hybridization of  $c = 5 \text{ nM}$  of WT target DNA for the indicated sensors. WT target was mixed 1:1 v:v with streptavidin coated magnetic beads and incubated over the sensor for  $30 \text{ min}$  at  $37 \text{ }^\circ\text{C}$ .



**Fig. 4.** Sensor signals from sensors functionalized with (a) WT probes, (b) biotinylated probes, (c) MT probes and (d) both WT and MT probes on the top and bottom halves of the sensor, respectively. (a,c,d) The signals were measured after 30 min hybridization with the biotinylated WT target mixed with streptavidin magnetic beads followed by washing and while ramping the temperature from 20 °C to 70 °C and back. (b) The signal was measured before and after bead binding to the biotinylated probes. Each curve shows the data obtained while ramping both up and down in temperature.

#### 4.2. Melting curve

A temperature ramping from 20 °C to 70 °C was employed to measure the melting curve on-chip. Fig. 4 shows the raw signal from the four sensors during the temperature ramping. The raw signals are useful to identify and discuss the temperature dependence of the sensor signal. Fig. 4b shows the signal of the positive reference sensor measured before and after binding of magnetic beads to the sensor surface. Each curve comprises a temperature ramp from 20 °C to 70 °C and back. Both measurements with and without beads proved to be reversible with complete overlap of data measured while the temperature was ramped up and down. The second harmonic out-of-phase signal offset (i.e., the sensor signal without magnetic beads) showed a small, non-linear increase with increasing temperature. Conversely, the bead signal decreased almost linearly with increasing temperature with a larger signal change with temperature. The reversibility of the bead signal during the downwards ramping of the temperature evidences that the strong biotin–streptavidin link is not broken in this range of temperatures. During the heating, there is no loss of magnetic particles from the positive reference sensor. Therefore the signal difference between the sweeps with and without beads ( $\Delta V_{\text{ref}}$ ) can be used to compensate for the temperature dependence of the low-field sensitivity  $S_0(T)$ .

Fig. 4a, c and d show the signals from WT, MT and WT–MT sensors, respectively. The signals were measured after hybridization while increasing the temperature from 20 °C to 70 °C and immediately after while decreasing the temperature back to 20 °C. For the WT and MT sensors (Fig. 4a and c) the signals first decreased linearly with temperature at low temperatures followed by an abrupt signal decrease at  $T \approx 45$  °C and  $T \approx 35$  °C for the WT

and MT sensors, respectively. This signal loss is consistent with the melting of DNA hybrids and therefore with magnetic beads detaching from the sensor surface. At high temperatures the signals stabilized at low values. During the reversed temperature ramp from 70 °C to 20 °C the signals remained at low values but showed a non-linear temperature dependence. The signals measured while ramping the temperature down characterize the temperature dependence of the signal offset and are used to calculate the bead signal  $\Delta V(T)$ .

Fig. 4d shows the signal from the sensor functionalized with both the WT and MT capture probes (WT–MT sensor). The signal measured while ramping the temperature up increased at  $T \approx 35$  °C, reached a maximum at  $T \approx 40$  °C and decreased at  $T \approx 45$  °C, which is consistent with the difference between the signals from the WT and MT sensors. Fig. 5 shows the relative signals obtained for the WT, MT and WT–MT sensors using the data correction procedure described in Section 3.5. The relative signal for the three sensors was constant at low temperature ( $T < 30$  °C). The relative signal for the WT sensor was notably higher than that for the MT sensor. The signals from the WT and MT sensors decreased in the middle temperature range and approached zero for  $T > 60$  °C. The relative signals for the MT and WT sensors dropped in the range  $T = 30$ –40 °C and  $T = 40$ –50 °C, respectively. Error function fits to the melting profile reveal melting temperatures of  $T_m = 35(1)$  °C for the MT sensor and  $T_m = 43(1)$  °C for the WT sensor, respectively. These numbers were obtained from triplicate experiments (standard deviations given in parentheses) and correspond to the temperatures where half of the signal has decayed. The signal from the sensor decreases when DNA hybrids are denatured and therefore magnetic labels are re-dispersed in the fluid, away from the sensor. The melting of the

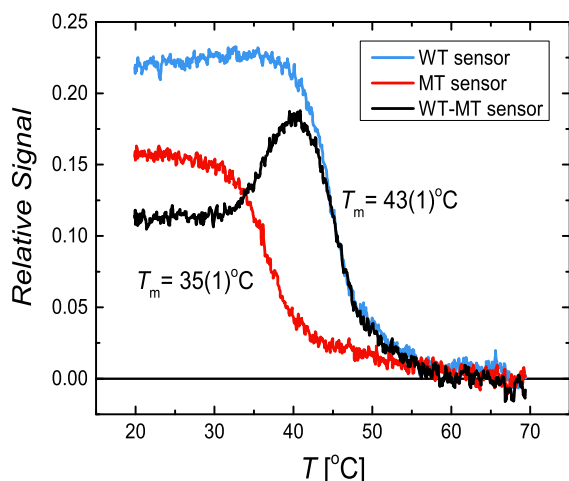


**Fig. 5.** Relative signal measured during a temperature ramp from 20 °C to 70 °C. Three sensors were measured simultaneously. Melting temperatures  $T_m$  were obtained from error function fits ( $n=3$ ). Numbers in parentheses give the standard deviations.

less stable non-complementary hybrids (WT target MT probes) occurred at a temperature 8 °C lower than the perfectly matched WT target WT probe hybrids. In the investigated temperature window, the optimal conditions to genotype the target mutation are for  $T = 35\text{--}43$  °C.

The relative signal for the WT–MT sensor correctly follows the difference between the signals from the other two sensors, in particular it shows a peak for  $T \approx 40$  °C where the difference between the signal from WT and MT sensor is maximum. The presence of a maximum indicates a stronger link of the target to the WT probe. The use of two probes on the same sensor allows to increase the number of investigated mutations on the same chip.

The use of surface bound probes allows to combine the power of melting analysis and the throughput of multiplexed assays. Other systems for array based denaturation studies have been developed for the purpose such as multithermal microarray washers [22], surface plasmon resonance (SPR) based detection [24] and membrane-based dynamic allele-specific hybridization (DASH) systems [25,26]. The system presented in this work has the potential advantage of employing magnetic particles as labels. The magnetic particles are stable over time and temperature and allow to measure the signal independently from the sample matrix. The magnetic readout allows to measure the hybridization signal in real-time during a continuous change of the conditions.

## 5. Conclusion

A system for melting curve measurement of surface tethered DNA hybrids was presented. For the first time, a magnetoresistive sensor was applied to the detection of DNA binding and thermal denaturation by using magnetic labels. The system provides a general tool to study the solid-surface hybridization kinetics in a DNA-chip format. The results of such studies are of greater interest since they could be applied to improve the more common DNA microarray analysis. Our sensor design and measurement setup are scalable. The present work represents the first step towards a system combining large arrays of magnetoresistive sensors with melting curve analysis. Such a system could be employed in genotyping tasks where there is a requirement for highly specific detection of multiple genetic markers, such as for cancer diagnostics.

## Acknowledgments

This work was supported by Copenhagen Graduate School for Nanoscience and Nanotechnology (C:O:N:T), the Knut and Alice Wallenberg (KAW) Foundation and the Danish Council for Independent Research (DFR-4005-00116).

## References

- [1] G. Reiss, H. Brueckl, A. Huetten, J. Schotter, M. Brzeska, M. Panhorr, D. Sudfeld, A. Becker, P.B. Kamp, A. Puehler, K. Wojczykowski, P. Jutzi, Magnetoresistive sensors and magnetic nanoparticles for biotechnology, *J. Mater. Res.* 20 (2005) 3294–3302. <http://dx.doi.org/10.1557/jmr.2005.0409>.
- [2] P.P. Freitas, R. Ferreira, S. Cardoso, F. Cardoso, Magnetoresistive sensors, *J. Phys.: Condens. Matter* 19 (16) (2007) 165221. <http://dx.doi.org/10.1088/0953-8984/19/16/165221>.
- [3] C. Tamanaha, S. Mulvaney, J. Rife, L. Whitman, Magnetic labeling, detection, and system integration, *Biosens. Bioelectron.* 24 (1) (2008) 1–13. <http://dx.doi.org/10.1016/j.bios.2008.02.009>.
- [4] S.X. Wang, G. Li, Advances in giant magnetoresistance biosensors with magnetic nanoparticle tags: review and outlook, *IEEE Trans. Magn.* 44 (7) (2008) 1687–1702. <http://dx.doi.org/10.1109/TMAG.2008.920962>.
- [5] D. Issadore, Y.I. Park, H. Shao, C. Min, K. Lee, M. Liong, R. Weissleder, H. Lee, Magnetic sensing technology for molecular analyses, *Lab Chip* 14 (2014) 2385–2397. <http://dx.doi.org/10.1039/C4LC00314D>.
- [6] R.D. Canales, Y. Luo, J.C. Willey, B. Austermiller, C.C. Barbacioru, C. Boysen, K. Hunkapiller, R.V. Jensen, C.R. Knight, K.Y. Lee, Y. Ma, B. Maqsoodi, A. Papallo, E.H. Peters, K. Poulter, P.L. Ruppel, R.R. Samaha, L. Shi, W. Yang, L. Zhang, F.M. Goodsaid, Evaluation of DNA microarray results with quantitative gene expression platforms, *Nat. Biotechnol.* 24 (9) (2006) 1115–1122. <http://dx.doi.org/10.1038/nbt1236>.
- [7] M. Dufva, J. Petersen, L. Poulsen, Increasing the specificity and function of dna microarrays by processing arrays at different stringencies, *Anal. Bioanal. Chem.* 395 (3) (2009) 669–677. <http://dx.doi.org/10.1007/s00216-009-2848-z>.
- [8] R.S. Gaster, L. Xu, S.J. Han, R.J. Wilson, D.A. Hall, S.J. Osterfeld, H. Yu, S.X. Wang, Quantification of protein interactions and solution transport using high-density GMR sensor arrays, *Nat. Nanotechnol.* 6 (5) (2011) 314–320. <http://dx.doi.org/10.1038/NNANO.2011.45>.
- [9] R.S. Gaster, D.A. Hall, S.X. Wang, nanolab: an ultraportable, handheld diagnostic laboratory for global health, *Lab Chip* 11 (5) (2011) 950–956. <http://dx.doi.org/10.1039/C0LC00534G>.
- [10] L. Xu, H. Yu, M.S. Akhras, S.-J. Han, S. Osterfeld, R.L. White, N. Pourmand, S.X. Wang, Giant magnetoresistive biochip for dna detection and hpv genotyping, *Biosens. Bioelectron.* 24 (1) (2008) 99–103. <http://dx.doi.org/10.1016/j.bios.2008.03.030>.
- [11] R. Edelstein, C. Tamanaha, P. Sheehan, M. Miller, D. Baselt, L. Whitman, R. Colton, The BARC biosensor applied to the detection of biological warfare agents, *Biosens. Bioelectron.* 14 (10–11) (2000) 805–813. [http://dx.doi.org/10.1016/S0956-5663\(99\)00054-8](http://dx.doi.org/10.1016/S0956-5663(99)00054-8).
- [12] B. de Boer, J. Kahlman, T. Jansen, H. Duric, J. Veen, An integrated and sensitive detection platform for magneto-resistive biosensors, *Biosens. Bioelectron.* 22 (9–10) (2007) 2366–2370. <http://dx.doi.org/10.1016/j.bios.2006.09.020>.
- [13] D.L. Graham, H. Ferreira, J. Bernardo, P.P. Freitas, J.M.S. Cabral, Single magnetic microsphere placement and detection on-chip using current line designs with integrated spin valve sensors: biotechnological applications, *J. Appl. Phys.* 91 (10) (2002) 7786–7788. <http://dx.doi.org/10.1063/1.1451898>.
- [14] G. Li, V. Joshi, R.L. White, S.X. Wang, J.T. Kemp, C. Webb, R.W. Davis, S. Sun, Detection of single micron-sized magnetic bead and magnetic nanoparticles using spin valve sensors for biological applications, *J. Appl. Phys.* 93 (10) (2003) 7557–7559. <http://dx.doi.org/10.1063/1.1540176>.
- [15] W. Shen, X. Liu, D. Mazumdar, G. Xiao, In situ detection of single micron-sized magnetic beads using magnetic tunnel junction sensors, *Appl. Phys. Lett.* 86 (25) (2005) 253901. <http://dx.doi.org/10.1063/1.1952582>.
- [16] G. Rizzi, F.W. Østerberg, M. Dufva, M.F. Hansen, Magnetoresistive sensor for real-time single nucleotide polymorphism genotyping, *Biosens. Bioelectron.* 52 (2014) 445–451. <http://dx.doi.org/10.1016/j.bios.2013.09.026>.
- [17] T.B.G. Hansen, C.D. Damsgaard, B.T. Dalslet, M.F. Hansen, Theoretical study of in-plane response of magnetic field sensor to magnetic beads magnetized by the sensor self-field, *J. Appl. Phys.* 107 (12) (2010) 124511. <http://dx.doi.org/10.1063/1.3366717>.
- [18] F.W. Østerberg, G. Rizzi, M.F. Hansen, On-chip measurements of Brownian relaxation of magnetic beads with diameters from 10 nm to 250 nm, *J. Appl. Phys.* 113 (15) (2013) 154507. <http://dx.doi.org/10.1063/1.4802657>.
- [19] F.W. Østerberg, G. Rizzi, A.D. Henriksen, M.F. Hansen, Planar hall effect bridge geometries optimized for magnetic bead detection, *J. Appl. Phys.* 115 (18) (2014) 184505. <http://dx.doi.org/10.1063/1.4876256>.
- [20] G. Rizzi, N.C. Lundtoft, F.W. Østerberg, M.F. Hansen, Reversible and irreversible temperature-induced changes in exchange-biased planar Hall effect bridge (PHEB) magnetic field sensors, *Sensor Transducers J.* 15 (2012) 22.
- [21] A.D. Henriksen, B.T. Dalslet, D.H. Skieller, K.H. Lee, F. Okkels, M.F. Hansen, Planar Hall effect bridge magnetic field sensors, *Appl. Phys. Lett.* 97 (1) (2010) 013507. <http://dx.doi.org/10.1063/1.3460290>.

- [22] J. Petersen, L. Poulsen, S. Petronis, H. Birgens, M. Dufva, Use of a multi-thermal washer for dna microarrays simplifies probe design and gives robust genotyping assays, *Nucleic Acids Res.* 36 (2) (2008) e10. <http://dx.doi.org/10.1093/nar/gkm1081>.
- [23] F.W. Østerberg, B.T. Dalslet, D. Snakenborg, C. Johansson, M.F. Hansen, Chip-based measurements of Brownian relaxation of magnetic beads using a planar hall effect magnetic field sensor, *AIP Conference Proceedings* 1311, 2010, 176–183, <http://dx.doi.org/10.1063/1.3530009>.
- [24] J. Fiche, A. Buhot, R. Calemczuk, T. Livache, Temperature effects on DNA chip experiments from surface plasmon resonance imaging: isotherms and melting curves, *Biophys. J.* 92 (3) (2007) 935–946. <http://dx.doi.org/10.1529/biophysj.106.097790>.
- [25] M. Jobs, W.M. Howell, L. Strömqvist, T. Mayr, A.J. Brookes, Dash-2: flexible, low-cost, and high-throughput snp genotyping by dynamic allele-specific hybridization on membrane arrays, *Genome Res.* 13 (5) (2003) 916–924. <http://dx.doi.org/10.1101/gr.801103>.
- [26] L.S. Meuzelaar, K. Hopkins, E. Liebana, A.J. Brookes, DNA diagnostics by surface-bound melt-curve reactions, *J. Mol. Diagn.* 9 (1) (2007) 30–41. <http://dx.doi.org/10.2353/jmoldx.2007.060057>.